Convergent tracer tests in multilayered aquifers: The importance of vertical flow in the injection borehole

Riley, Michael; Tellam, John; Greswell, Richard; Durand, V; Aller, MF

DOI:
10.1029/2010WR009838

Convergent tracer tests in multilayered aquifers: The importance of vertical flow in the injection borehole

Michael S. Riley,[1] John H. Tellam,[1] Richard B. Greswell,[1] Véronique Durand,[1,2] and Maria F. Aller[1,3]

Received 31 July 2010; revised 15 April 2011; accepted 27 April 2011; published 1 July 2011.

[1] A mathematical model describing the steady state flows in a forced gradient tracer test between an injection and pumping borehole in a multilayered sandstone aquifer has been developed that includes the effect of vertically variable background heads. A second model describing the recovery of tracer from a layer in which there are discharges due to vertical flow in the injection borehole is also presented. Application of the models to field tracer test data indicates that the observed recoveries, which are not proportional to the abstraction rate in each layer, are consistent with the hydraulic behavior of the aquifer when natural vertical head gradients are taken into account. Investigation with the models illustrates that the vertical distribution of tracer recovery depends strongly upon the background heads and that tracer tests conducted in the same aquifer, but at different times, may interrogate different aquifer layers. It is also shown generally that for a given abstraction rate the vertical distribution of tracer recovery in small-scale tracer tests is controlled largely by the transmissivity distribution but that as the spatial scale of the test increases, the distribution of recovery becomes proportional to the discharges from the injection borehole because of vertical flows within it, which may be natural or induced by pumping in the monitoring borehole. Uncertainties inherent in the design of forced gradient tracer tests in multilayered aquifers and the problems of applying the results of such tests to natural gradient contaminant migration are discussed.

Citation: Riley, M. S., J. H. Tellam, R. B. Greswell, V. Durand, and M. F. Aller (2011), Convergent tracer tests in multilayered aquifers: The importance of vertical flow in the injection borehole, *Water Resour. Res.*, *47*, W07501, doi:10.1029/2010WR009838.

1. Introduction

[2] Forced gradient tracer tests between an injection and a pumping borehole are used often in experimental investigations into the transport properties of contaminants and aquifers [*Ptak et al.*, 2004], and recently, they have been used to evaluate subsurface heat transport [e.g., *Clarkson et al.*, 2009]. This paper is concerned with tests in which the introduction of tracer is achieved without significant modification of the flow field around the injection well [e.g., *Lloyd et al.*, 1996; *Ptak and Schmid*, 1996; *McCarthy et al.*, 1996; *Gutiérrez et al.*, 1997; *Karasaki et al.*, 2000; *Riley et al.*, 2001; *Streetly et al.*, 2002; *Reimus et al.*, 2003a; *Reimus et al.*, 2003b; *Kurtzman et al.*, 2005; *Gierczak et al.*, 2006; *Mathias et al.*, 2007; *Hartmann et al.*, 2007; *Joyce et al.*, 2008; *Taylor et al.*, 2010]. In particular, we concentrate on multilayered systems composed of a sequence of aquifer units separated by aquitards. Such systems may exhibit variations in head over depth, with vertical flow inhibited by the aquitard layers. An injection borehole constructed in such a system will act as a conduit for vertical flow, which will affect the delivery of tracer to each aquifer layer, and consequently, the vertical distribution of tracer recovery. Even where vertical gradients are not present naturally, abstraction from the pumping (monitoring) borehole will induce vertical flows in the injection borehole if the aquifer hydraulic properties are depth dependent. The importance of the spatial variation of inflow to the aquifer from the injection borehole on the interpretation of a tracer test has long been recognized and methods, typically based on point dilution techniques, have been employed in the field to estimate the distribution [e.g., *Ronen et al.*, 1991; *Flynn et al.*, 2005; *West and Odling* 2007; *Mathias et al.*, 2007]. Of interest here is the quantification of the vertical distribution of tracer delivery to the aquifer, including the impact of vertical flow in the injection borehole, from the hydraulic properties of the aquifer and the pumping rate in the abstraction borehole. We present general formulae describing the steady state heads and flows in both boreholes due to background head gradients modified by pumping, and a description of the theoretical mass recovery in each layer. These models are applied to the results of a tracer test conducted with novel

[1]Water Sciences, School of Geography, Earth and Environmental Sciences, University of Birmingham, Birmingham, UK.
[2]Now at Laboratoire Interactions et Dynamique des Environnements de Surface, UMR 8148, Université Paris–Sud XI, CNRS, Orsay, France.
[3]Now at Centre for Sustainable Water Management, Lancaster Environment Centre, Lancaster, UK.

0043-1397/11/2010WR009838

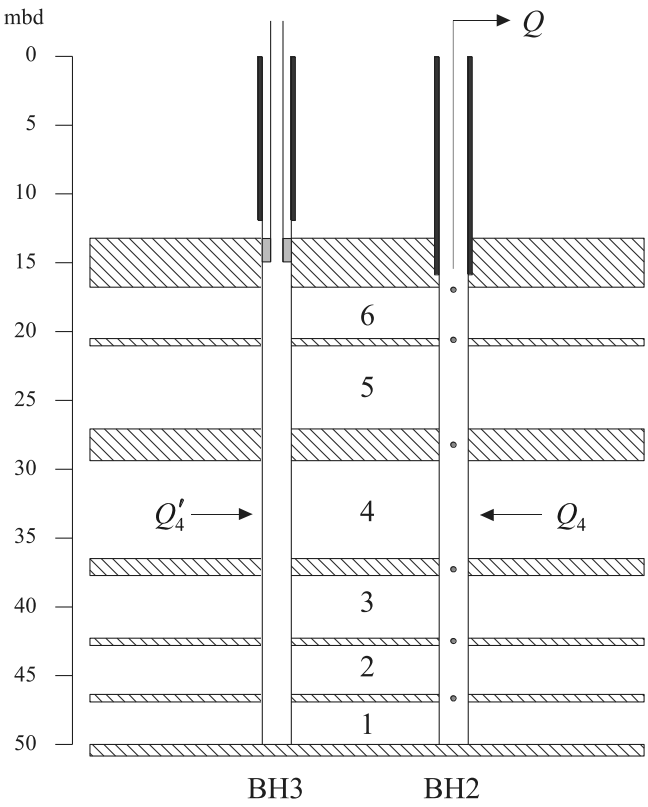

Figure 1. Conceptual model of aquifer and schematic tracer test setup. Hatched regions are aquitards; numbers 1–6 are the layer numbers referred to in the text; circles give the sampling positions; solid black rectangles represent the cased sections of each borehole; gray rectangles represent the inflatable packer, which is connected to the surface with a flexible pipe. Discharges to each borehole are shown for layer 4 to illustrate the sign convention employed.

monitoring in a multilayered aquifer system. We investigate how mass recovery over depth is affected by changes in background heads, explore the effect of the scale of the test, and consider the sensitivity of tracer recovery to the hydraulic regime close to the injection borehole. Finally, we consider the implications for tracer test interpretation and design.

2. Hydraulics and Tracer Recovery

2.1. Steady State Hydraulics of a Pair of Boreholes in a Multilayered Aquifer

[3] Here we consider the steady state hydraulics of a tracer test conducted between an injection and an abstraction borehole in a multilayered aquifer (Figure 1), and present formulae describing the heads in each borehole and flows to and from them. We assume that the aquifer is composed of N laterally homogeneous and isotropic aquifer units confined by laterally extensive aquitards (effectively aquicludes), and that each aquifer unit is penetrated to the same extent by the boreholes. The steady state background heads, namely, those at distance from the borehole, may be different in each layer. The pump in the abstraction borehole is located either within the top aquifer layer or in the casing above, and we assume that upflow losses in the borehole are negligible.

[4] For a particular aquifer layer, the steady state drawdown in each borehole is given simply by superposing Thiem equations. For the pumped and injection boreholes, the resulting equations for layer n are

$$H_n - h_w = \frac{Q_n}{2\pi T_n}\ln\left(\frac{R_n}{r_w}\right) + \frac{Q'_n}{2\pi T_n}\ln\left(\frac{R'_n}{r}\right) \tag{1}$$

$$H_n - h'_w = \frac{Q_n}{2\pi T_n}\ln\left(\frac{R_n}{r}\right) + \frac{Q'_n}{2\pi T_n}\ln\left(\frac{R'_n}{r'_w}\right), \tag{2}$$

respectively, where H_n $[L]$ is the background head, h_w and h'_w $[L]$ are the heads in the abstraction and injection borehole, respectively, Q_n $[L^3\ T^{-1}]$ is the outflow from the aquifer at the abstraction borehole due to the combined effect of pumping and vertical head gradients, Q'_n $[L^3\ T^{-1}]$ is the outflow from the aquifer at the injection borehole due to vertical flow in the borehole, T_n $[L^2\ T^{-1}]$ is the layer transmissivity, R_n $[L]$ is the radius of influence of the discharge to the abstraction well, and R'_n $[L]$ is the radius of influence of the discharge to the injection well due to vertical flow, r_w and r'_w $[L]$ are the radii of the abstraction and injection boreholes, respectively, and r $[L]$ is the distance between borehole centers.

[5] The mass balance equations are constructed by noting that the upflow in a borehole through an aquitard, $Q_{V,n+1}$ $[L^3\ T^{-1}]$, is given by the upflow in the borehole through the aquitard immediately below plus the inflow from the intervening aquifer layer. Thus, for all n,

$$Q_{V,n+1} = Q_{V,n} + Q_n \tag{3}$$

$$Q'_{V,n+1} = Q'_{V,n} + Q'_n, \tag{4}$$

where the prime indicates the injection borehole. We assume that there is no vertical flow into the bottom of either borehole, nor flow out of the top of the injection borehole. Hence,

$$Q_{V,0} = Q'_{V,0} = Q'_{V,N} = 0. \tag{5}$$

Discharge from the pumping borehole, Q $[L^3\ T^{-1}]$, occurs at the top of the borehole and so

$$Q_{V,N} = Q. \tag{6}$$

Solving equations (1)–(6) gives heads in the pumped and observation wells as

$$h_w = \frac{2\pi\left(\sum_{i=1}^{N} T_i\right)\sum_{i=1}^{N}\left(\frac{T_i}{\mu_i}H_i\right) - Q\sum_{i=1}^{N}\left(\frac{T_i}{\mu_i}\ln\left(\frac{R_i}{r_w}\right)\right)}{2\pi\left(\sum_{i=1}^{N} T_i\right)\sum_{i=1}^{N}\left(\frac{T_i}{\mu_i}\right)} \tag{7}$$

$$h'_w = \frac{2\pi\left(\sum_{i=1}^{N} T_i\right)\sum_{i=1}^{N}\left(\frac{T_i}{\mu_i}H_i\right) - Q\sum_{i=1}^{N}\left(\frac{T_i}{\mu_i}\ln\left(\frac{R_i}{r}\right)\right)}{2\pi\left(\sum_{i=1}^{N} T_i\right)\sum_{i=1}^{N}\left(\frac{T_i}{\mu_i}\right)}, \tag{8}$$

respectively, where

$$\mu_i = \ln\left(\frac{R_i}{r_w}\right)\ln\left(\frac{R_i'}{r_w'}\right) - \ln\left(\frac{R_i}{r}\right)\ln\left(\frac{R_i'}{r}\right). \quad (9)$$

Drawdown is given simply by the difference between the head at zero discharge and that during pumping. So the drawdown in each borehole is given by

$$s_w = \frac{Q\sum_{i=1}^{N}\left(\frac{T_i}{\mu_i}\ln\left(\frac{R_i}{r_w}\right)\right)}{2\pi\left(\sum_{i=1}^{N}T_i\right)\sum_{i=1}^{N}\left(\frac{T_i}{\mu_i}\right)} \quad (10)$$

$$s_w' = \frac{Q\sum_{i=1}^{N}\left(\frac{T_i}{\mu_i}\ln\left(\frac{R_i}{r}\right)\right)}{2\pi\left(\sum_{i=1}^{N}T_i\right)\sum_{i=1}^{N}\left(\frac{T_i}{\mu_i}\right)}. \quad (11)$$

The lateral flows to the pumped and observation boreholes in layer n are

$$Q_n = \frac{2\pi T_n}{\mu_n}\left[H_n\ln\left(\frac{r}{r_w'}\right) + h_w'\ln\left(\frac{R_n'}{r}\right) - h_w\ln\left(\frac{R_n'}{r_w'}\right)\right] \quad (12)$$

$$Q_n' = \frac{2\pi T_n}{\mu_n}\left[H_n\ln\left(\frac{r}{r_w}\right) + h_w\ln\left(\frac{R_n}{r}\right) - h_w'\ln\left(\frac{R_n}{r_w}\right)\right], \quad (13)$$

respectively.

2.2. Theoretical Mass Recovery

[6] In this section we consider the recovery of a nonreactive tracer in each layer at the pumping borehole. Hydrodynamic dispersion and ambient horizontal groundwater flow are assumed to be negligible and the boreholes to be parallel. The mass of tracer transferred from the injection borehole to an aquifer layer depends upon the pumping rate in that layer and the flows to or from the injection borehole due to vertical flow. Mass recovery in layer n requires $Q_n > 0$ and is further controlled by the location of the flow stagnation point created by the discharges from the two boreholes. If the radius of the boreholes were effectively zero, a stagnation point would exist along the line joining the borehole centers at a distance $rQ_n'/(Q_n + Q_n')$ from the center of the injection borehole. However, the existence of a finite radius borehole can distort (in many cases, focus) the horizontal flow field, thereby modifying the location of the stagnation point in the region of the borehole. For the case in which the stagnation point is close to the injection borehole, i.e., when $|Q_n'| \ll Q_n$, the distance of the stagnation point from its center, measured toward the abstraction borehole, can be approximated by $rQ_n'/(\alpha_n Q_n + Q_n')$, where α_n is a dimensionless focusing factor. It is convenient for later discussion to define the dimensionless number

$$\Omega_n = \frac{rQ_n'}{r_w'(\alpha_n Q_n + Q_n')}, \quad (14)$$

which characterizes the location of the stagnation point such that it lies within the injection borehole when $-1 < \Omega_n < 1$.

[7] From the symmetry of the geometry of the test setup, when $|Q_n'| \gg Q_n$, the stagnation point is close to the abstraction borehole and its distance from the center of the borehole in the direction of the injection borehole can be approximated by $rQ_n/(\alpha_n Q_n' + Q_n)$. Here, to avoid complicating the notation, we have assumed that the focusing factor is the same for each borehole, but a simple, appropriate substitution can remove this assumption if necessary.

[8] In general, the stagnation point can lie within one of five distinct regions, each of which leads to a different regime of tracer recovery. These regions are demarcated by values of Q_n'/Q_n derived simply from the expressions for the locations of the stagnation points given in the preceding paragraph. These regions, in order of decreasing values of Q_n'/Q_n (i.e., from large positive to large negative values of Q_n') are (1) between the center of the abstraction borehole and the rim of the injection borehole closest to the abstraction borehole, (2) within the injection borehole, (3) outside the injection borehole, on the opposite side from the abstraction borehole, (4) outside the abstraction borehole on the far side from the injection borehole, and (5) within the abstraction borehole on the far side of the center from the injection borehole.

[9] We introduce a recovery function, $f(Q_n', Q_n)$, defined as that discharge of water from the injection borehole that is captured at the abstraction borehole.

[10] In case 1, the injection borehole is not within the capture zone of the abstraction borehole and so the recovery function is zero.

[11] It is convenient to consider case 3 before case 2. In case 3, the whole of the injection borehole is within the capture zone of the abstraction borehole and so the value of the recovery function is equal to the discharge from the injection borehole to layer n of the aquifer ($-Q_n'$).

[12] In case 2, the theoretical stagnation point lies within the injection borehole. Locating a stagnation point within the borehole presupposes that Q_n' can be represented by a point sink (Figure 2a). However, if Q_n' is, a little more realistically, considered to be uniformly distributed across the borehole, no such stagnation point exists (Figure 2b). Nevertheless, since the permeability within the borehole is generally many times larger than that of the rock, both models produce effectively the same pattern of flow outside the borehole (Figure 2), and so we can extend the use of a theoretical stagnation point to within the borehole to characterize the flow around it.

[13] In case 2, the recovery function varies continuously with Q_n' and Q_n. We are not aware of an analytical expression for the recovery function in this case and so numerical experiments were conducted, using COMSOL Multiphysics, to assess its dependence on Q_n' for fixed values of Q_n. Values of the recovery function were estimated for a range of values of Q_n' by integrating the normal flux from the injection borehole over that part of its rim from which outflow is captured by the abstraction borehole. The evidence is strong that this function can be approximated well by a quadratic in Q_n'. For parameter values: $r/r_w' = 20$, $\alpha_n = 2$ and $Q_n = 1$; the value of R^2 from the least squares quadratic fit is 1.0 (to 3 decimal places). A similarly good fit was achieved using the geometry and abstraction rate from the tracer test described in section 3. The exact form and coefficients of this quadratic function, $g(Q_n', Q_n)$, can be established algebraically from three known

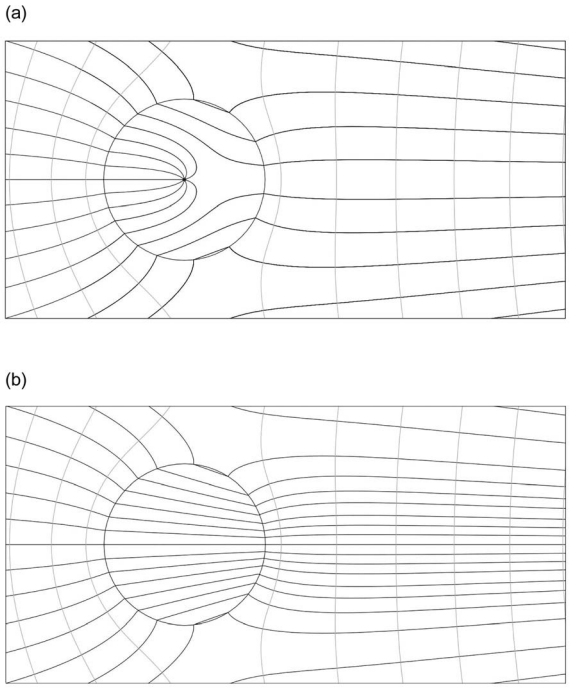

Figure 2. Streamlines and equipotentials in and around the injection borehole simulated using COMSOL Multiphysics when Q'_n is treated as (a) a point sink and (b) a distributed sink. The abstraction borehole (not shown) is located to the right of the injection borehole; $\Omega_n = 0.3$, $r/r'_w = 20$, $\alpha_n = 2$, and $Q_n = 1$.

pairs of values of Ω_n and $g(Q'_n, Q_n)$ determined from the two stagnation points on the rim of the borehole [$\Omega_n = -1$, $g(Q'_n, Q_n) = -Q'_n$; and $\Omega_n = 1$, $g(Q'_n, Q_n) = 0$] and from the case in which the discharge due to vertical flow is zero [$\Omega_n = 0$, $g(Q'_n, Q_n) = r'_w\alpha_n/\pi r$]. This gives

$$g(Q'_n, Q_n) = \frac{aQ'^2_n + bQ'_nQ_n + cQ^2_n}{Q_n}, \tag{15}$$

where

$$a = \frac{(\pi - 2)\left(r^2 - r'^2_w\right)}{2\pi r r'_w \alpha_n}, \quad b = \frac{(4 - \pi)r'_w - \pi r}{2\pi r}, \quad c = \frac{r'_w\alpha_n}{\pi r}. \tag{16}$$

Figure 3 shows the simulated recovery function and the quadratic model against Q'_n for parameter values: $r/r'_w = 20$, $\alpha_n = 2$ and $Q_n = 1$.

[14] As the value of Q'_n becomes more negative than $-Q_n$, the stagnation point switches to the opposite side of the abstraction borehole from the injection borehole (case 4). In this case, all the water abstracted originates from the injection borehole and so the recovery function is equal to Q_n.

[15] Finally, in case 5, as Q'_n becomes sufficiently negative, the stagnation point moves inside that part of the abstraction borehole on the far side from the injection borehole. A stagnation point at the center of the abstraction borehole represents a zero abstraction and hence a recovery of zero. Thus, in case 5 the recovery function varies continuously between Q_n at the borehole rim and zero at the center according to a function, $g_{abs}(Q'_n, Q_n)$. The exact form of the function $g_{abs}(Q'_n, Q_n)$ is of little practical interest here since it covers the transition between recovery function values of zero and Q_n, but applies only when Q_n is considerably smaller in magnitude than Q'_n and hence when the recovery is already close to zero.

[16] In summary, the fraction, m_n, of the total mass recovery that is retrieved from level n in the abstraction borehole, in a system with N layers is given by

$$m_n = \frac{f(Q'_n, Q_n)}{\sum_{i=1}^{N} f(Q'_n, Q_n)}, \tag{17}$$

where $f(Q'_n, Q_n)$ is zero if $Q_n \le 0$ and is otherwise defined by equation (18):

$$f(Q'_n, Q_n) = \begin{cases} 0 & \text{if} \quad \dfrac{\alpha_n r'_w}{r - r'_w} < \dfrac{Q'_n}{Q_n} \\ g(Q'_n, Q_n) & \text{if} \quad -\dfrac{\alpha_n r'_w}{r + r'_w} < \dfrac{Q'_n}{Q_n} < \dfrac{\alpha_n r'_w}{r - r'_w} \\ -Q_n & \text{if} \quad -1 < \dfrac{Q'_n}{Q_n} < -\dfrac{\alpha_n r'_w}{r + r'_w} \\ Q_n & \text{if} \quad -\dfrac{r + r_w}{\alpha_n r_w} < \dfrac{Q'_n}{Q_n} < -1 \\ g_{abs}(Q'_n, Q_n) & \text{if} \quad \dfrac{Q'_n}{Q_n} < -\dfrac{r + r_w}{\alpha_n r_w} \end{cases}. \tag{18}$$

3. Tracer Test

3.1. Background

[17] The tracer test was conducted in 2008 at the University of Birmingham, United Kingdom, in a Permo-Triassic Sandstone aquifer. This sandstone, described by

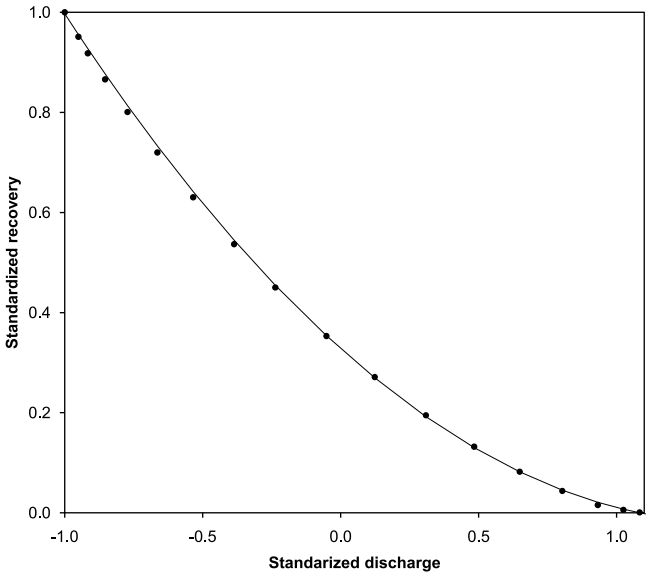

Figure 3. Simulated values of recovery (solid circles) and the quadratic model (solid line) as a function of Q'_n when $-1 < \Omega_n < 1$, $r/r'_w = 20$, $\alpha_n = 2$, and $Q_n = 1$. All values are standardized by the magnitude of Q'_n that corresponds to $\Omega_n = -1$.

Allen et al. [1997], *Tellam and Barker* [2006], and *Hitchmough et al.* [2007], is used extensively for water supply in England and underlies several other major cities, including Nottingham, Liverpool, and Manchester. The sequence investigated comprises weakly to well-cemented fluvial and aeolian sandstones, with occasional mudstones and paleosols.

[18] The test site comprises two closely spaced boreholes and a third approximately 20 m from both. Initial site characterization was carried out using optical televiewer, natural gamma and resistivity borehole logs; cores from the boreholes were lithologically described and extensively tested for permeability [*Bouch et al.*, 2006]. The tracer test reported below was designed as part of a sequence of investigations into the migration of viruses in the sandstone, in which fluorescein was used as nonreactive tracer.

3.2. Tracer Injection and Sampling

[19] The injection and abstraction boreholes are 7.53 m apart (center to center), have internal diameters of 0.15 m, and are both open to 50 m below datum (mbd), which is taken to be the top of casing in BH3, the injection borehole (Figure 1). BH3 is cased to 12.2 mbd and the monitoring borehole (BH2) cased to 15.4 mbd. Cross-hole packer testing [*Ferguson*, 2006] indicated that the section of BH3 above 15 mbd is effectively isolated hydraulically from BH2 except through BH3 itself. Hence, to simplify the experiment, the section above 15 mbd in BH3 was isolated from that below with an inflatable packer connected to the surface by flexible piping so that work could be carried out in the lower part of the borehole (Figure 1). Tracers were introduced into BH3, without changing the head, using a recirculation system with a Grundfos MP1 pump installed just below the packer and connected to a length of 25 mm id piping running from the pump to the surface and down to the bottom of the borehole. A tap for injection and sampling was inserted into the piping at the surface. A recirculation rate of 26 m^3 d^{-1}, which is sufficient to flush the borehole in about 30 min, was maintained until the concentration in the borehole was negligible.

[20] Abstraction from BH2 was achieved using a 3 inch Grundfos submersible pump with electronic speed control and a maximum discharge of 180 L min^{-1}, installed near the bottom of the casing. The system was pumped to steady state at 122 m^3 d^{-1}, after which 20 g of fluorescein dissolved in 10 L of water were injected into BH3 over a period of 95 min. A suspension of bacteriophages was injected approximately 24 h later. The test was monitored for 26 days. The heads above and below the packer in BH3 and in BH2 were monitored with Keller pressure transducers. Head monitoring started before the packer in BH3 was inflated and continued until the end of the test.

3.3. Tracer Sampling

[21] A novel sampling system, designed to collect water from discrete depths, was installed in BH2 below the 3 inch pump. This consisted of a single Grundfos MP1 pump encased in a pump chamber with a manifold at the bottom connected to 5 intake pipes, each one cut to sample at a selected depth in the borehole. Each intake pipe was connected to the manifold via a solenoid valve and a one-way valve. A similar system of pipes, one-way valves and manifold were fitted to the top of the pump chamber, the pipes leading to sampling points at the ground surface. The solenoid valves were controlled to route flow from each depth sequentially, through the pump and to a monitoring point at the surface for periods of 20 min at a time. Discharge from each sampling pipe (on average 5 m^3 d^{-1}) was fed through an Argonide NanoCeram® virus filter trap, with a small discharge taken from the sampling pipe at ground surface, using a peristaltic pump, and delivered to a Schnegg fluorimeter and to a particle counter. The virus traps were replaced daily, while fluorescein concentrations were logged every 10 s. A sample of the discharge from the 3 inch pump was passed continuously through a virus trap and another sample routed through a second fluorimeter.

[22] Samples were taken from depths of 16.2 mbd (through the 3 inch pump) and 21.5, 28.0, 38.4, 43.0, and 47 mbd through the Grundfos MP1 (Figure 1). The sampling depths were chosen to coincide with low-permeability layers determined from geophysical logs, borehole flow tests (section 3.4) and cross-hole packer testing [*Ferguson*, 2006], and define six aquifer layers numbered sequentially from the bottom of the system (Figure 1). Layer 1 is assumed to be bounded below by an aquitard close to the bottom of the boreholes. The low-permeability layers are either mudstones or paleosols [*Bouch et al.*, 2006; *Tellam and Barker*, 2006].

3.4. Borehole Flow Tests

[23] The recorded fluorescein concentrations represent the total inflow of tracer between the bottom of the borehole and each sampling level, and calculation of mass breakthrough in each layer requires the discharge at the abstraction borehole in each layer to be known. Estimates of these values were determined from the results of a borehole flow test, conducted after the tracer test [*Price*, 2008]. For this test, groundwater was abstracted using a pump installed inside the borehole casing. After steady state conditions were established, upflow was measured at a range of depths in the borehole using an impeller flowmeter installed inside a hollow-centered packer system. The cumulative inflow rates were then differentiated to give inflow per meter (Figure 4). The results closely match a similar test conducted before the tracer test, but at a coarser resolution.

3.5. Experimental Mass Recovery

[24] Unexpectedly, the mass of fluorescein recovered at each level during the test, expressed as a fraction of the total recovered (estimated to be 95% of that injected), was found not to be proportional to the abstraction rate in that level (Figure 5). Although this result could be attributable to nonradial flows caused by heterogeneity of the aquifer, measurements by *Ferguson* [2006] indicated an increase in head with depth at the experimental site, suggesting the possibility of significant vertical transport in the injection borehole, resulting in greater delivery of tracer to the upper layers of the aquifer. This appears to be consistent with the general trend of decreasing tracer recovery with depth. Such vertical head gradients are not uncommon in the UK Permo-Triassic sandstones [e.g., *Brassington*, 1992; *Segar*, 1993; *Rushton and Salmon*, 1993; *Stagg et al.*, 1998;

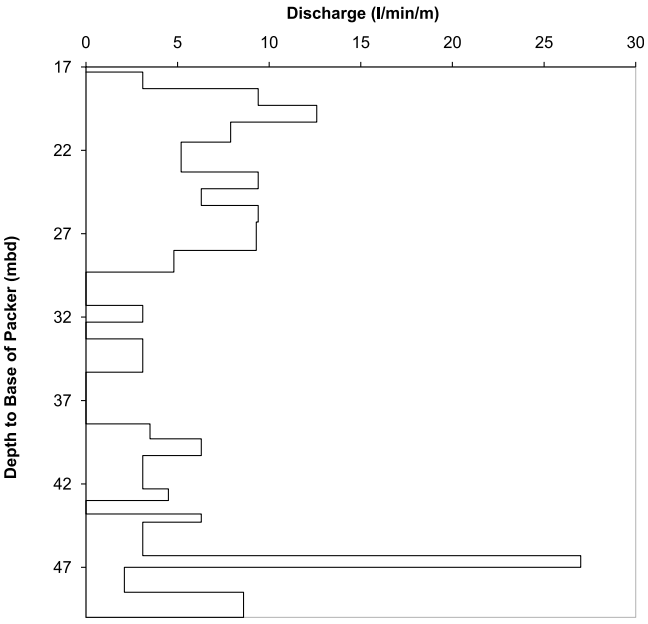

Figure 4. Inflow per unit length over depth in the abstraction and monitoring borehole.

Streetly et al., 2002; *Taylor et al.*, 2003; *Furlong et al.*, 2011].

4. Application of Theory to Field Data

4.1. Approach

[25] In this section, we test the feasibility of the hypothesis that the unexpected mass recovery in each layer is due to upflow in the system, particularly in the injection borehole. Taken together, the formulae presented in sections 2.1 and 2.2 describe the mass recovery in each layer as functions of the overall pumping rate in the abstraction borehole, and the transmissivity, radii of influence of abstractions and injections, and background head in each layer. Formulae for the drawdown in each borehole are also presented. Since the hydraulic properties of each layer are not well constrained by detailed field testing, the approach taken here is to use the mass recovery from the tracer test to estimate the hydraulic properties and to compare these with simply derived ranges of values for these parameters. In particular, the inferred radii of influence are compared with known limits on these values derived from monitored drawdown in other boreholes during the tracer and other hydraulic tests. Taking this approach requires the background heads in each layer to be known.

4.2. Determination of Background Heads

[26] The pattern of tracer recovery observed in the tracer test was unexpected and investigations to quantify the vertical head gradients were not conducted at the time of the test. However, in this section, we reanalyze work carried out in a different context at the site in 2006 in order to estimate the gradients. In the previous study, *Ferguson* [2006] conducted cross-hole packer tests in the experimental boreholes in which a single packer was installed at low-permeability horizons and the borehole pumped from above the packer with heads monitored above and below the packer and in the adjacent open hole (for details of the method, see *Le Borgne et al.* [2007]). As part of these tests, head changes above and below the packer were monitored during packer inflations and, additionally, an open hole constant rate discharge test was carried out. Step drawdown tests in the boreholes showed nonlinear losses in the pumping borehole to be insignificant for the abstraction rates used in the constant

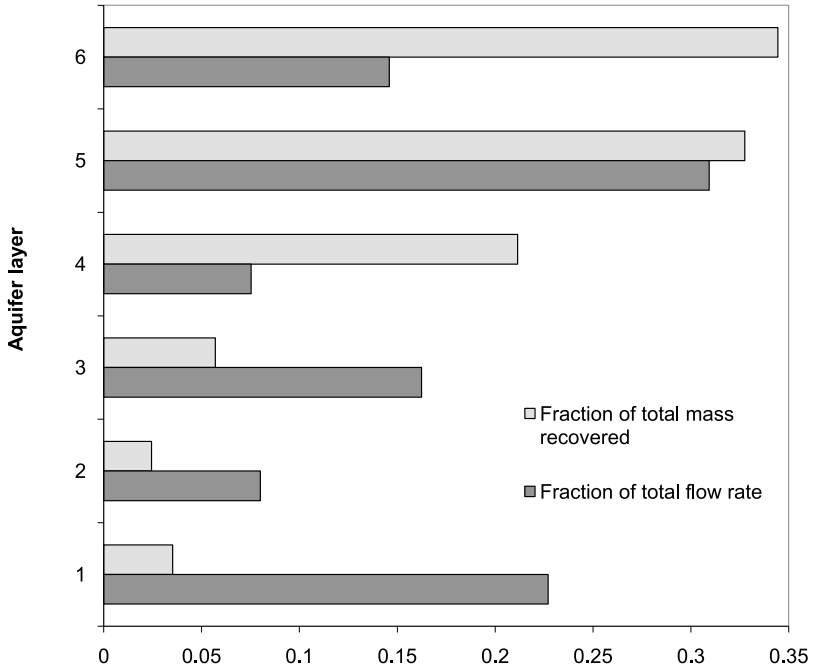

Figure 5. Fraction of total flow and tracer mass recovery at the monitoring borehole for each aquifer layer (tracer test conducted in 2008).

Table 1. Conductances (2006) and Background Heads (2006 and 2008)

	Aquifer Layer					
	1, 2	3	4	5	6	7[a]
C_n, 2006 (m^2 d^{-1})	5.3	4.4	2.8	8.8	7.6	23.5
H_n, 2006[b] (m)	2.15	1.82	0.68	0.66	−0.90	−0.86
H_n, 2008[b,c] (m)	0.098	0.087	0.050	0.049	−0.001	

[a]Layer 7 represents the aquifer overlying the test zone.
[b]Heads are given relative to the static water level in the open borehole at the start of the packer testing.
[c]Scaled head values assumed to apply during the tracer test.

discharge and tracer tests. In the analysis of the packer tests, the steady state flow to the borehole in any layer can be characterized by the product of a conductance term, C_i [L^2 T^{-1}], and a head difference, which has the advantage of requiring no assumptions to be made about the aquifer geometry. If, as in this study, the aquifer is assumed to comprise hydraulically distinct subhorizontal layers, the conductance term can be related simply to the parameters of the Thiem equation. If heads are measured relative to the initial static water level in the borehole, then when the hole is open and unpumped, the steady state mass balance equation is

$$\sum_{i=1}^{N} C_i H_i = 0. \tag{19}$$

When the packer is inflated at the top of layer n, the mass balance equations below and above the packer are

$$\sum_{i=1}^{n} C_i\left(H_i - \Delta h_{b,n}\right) = 0 \tag{20}$$

$$\sum_{i=n+1}^{N} C_i\left(H_i - \Delta h_{a,n}\right) = 0, \tag{21}$$

where $\Delta h_{b,n}$ and $\Delta h_{a,n}$ [L] are the increases in head observed on packer inflation below and above the packer, respectively. Finally, if the open borehole is pumped to steady state, the mass balance equation in the borehole is

$$\sum_{i=1}^{N} C_i(H_i - s) = Q, \tag{22}$$

where s [L] is the steady state drawdown in the borehole.

[27] Assuming the flow rate dependence of the conductances to be small, equations (19)–(22) can be solved simultaneously to give the conductances and background heads. Table 1 shows the results derived from tests conducted in 2006 in the injection borehole (BH3). Heads are presented relative to the static water level in the borehole when the packer tests were conducted. Note that in this set of tests, levels 1 and 2 from the tracer test were not differentiated. Under ambient conditions, layer 6 drains the aquifer. When the test zone was isolated from the overlying aquifer by an inflatable packer, the head below the packer increased by 0.68 m, changing the flow system in the test zone. Under these conditions, water enters the borehole from layers 1, 2, and 3 and exits through layers 5 and 6. There is no significant horizontal flow in layer 4.

[28] During the intervening period between the packer tests and the tracer test, the vertical head gradient at the site diminished markedly. During the packer inflations in the 2006 tests, the difference between the pressure monitored above and below the packer in the top position in BH3 was 1.54 m, whereas when the packer used in the tracer test, conducted in 2008, was inflated (in the same location) the differential pressure change was only 0.05 m. The reason for the significant change in heads is not understood. Generally, vertical flow in the aquifer in the region of the test site is thought to be caused by the Birmingham Fault, which juxtaposes the upper layers of the sandstone and substantial mudstone units, restricting horizontal regional flow and causing discharge to a stream approximately 200 m from the site. However, heads at the test site itself tend to be more complex with significant temporal variations. Since it was not practical to carry out detailed investigations into the ambient heads distribution following the 2008 test, the heads have had to be estimated. Thus, the heads (relative to the head in the overlying aquifer) that are assumed to apply during the tracer test have been derived by scaling the measured heads by the factor 0.05/1.54 (Table 1). Clearly, the derived head distribution is uncertain, but it is used in section 4.3 as the basis for an illustrative investigation into the nature and scale of the effect of vertical flow in the boreholes.

4.3. Hydraulic Properties Inferred From the Tracer and Hydraulic Tests

[29] In this section, we demonstrate that the discharges due to vertical flow in the injection borehole necessary to produce the observed mass recovery in each layer are consistent with the known hydraulic behavior of the aquifer.

[30] The approach taken is to use equations (9)–(13) and equations (15)–(18) to match the observed values of m_n, Q_n (for $n = 1 \ldots N$), s_w, and s'_w by varying the hydraulic properties, T_n, R_n, and R'_n. The values of H_n are modified from the work of *Ferguson* [2006] as described above, m_n, s_w, and s'_w are taken from the tracer test, and since the flow system is linear, values of Q_n can be inferred by scaling the results from the borehole flow tests (section 3.4) to match the pumping rate applied during the tracer test. Values of α_n are required, but are not simply determined and are likely to be affected by heterogeneities local to the injection borehole. As a first approximation, a single effective value was estimated for the entire open section of the injection borehole using the decrease in the tracer concentration, c [M L^{-3}], in the injection borehole and assuming that

$$\frac{dc}{dt} = -\lambda c, \tag{23}$$

where λ [T^{-1}] is given by the discharge through the injection borehole divided by the open borehole volume, from which

$$\alpha_n = \frac{\pi^2 r'^2_w r L \lambda}{Q} \tag{24}$$

for all n, where L [L] is the length of the open section of the borehole. When applied to the field data, this gives $\alpha_n = 1.0$.

Table 2. Mass Recovery, Flow to Boreholes, and Inferred Hydraulic Properties (2008)

	Aquifer Layer				
	1, 2	3	4	5	6
Fraction of mass recovered m_i	0.06	0.06	0.21	0.33	0.34
Abstraction rate Q_n (m^3 d^{-1})	38	20	9	38	18
Flow to injection borehole due to vertical flow Q'_n[a] (m^3 d^{-1})	0.239	0.086	−0.099	−0.065	−0.159
Ω_n	0.63	0.43	−1.10	−0.17	−0.90
Transmissivity T_n[a] (m^2 d^{-1})	7.45	3.93	1.85	7.55	3.60
Radius of influence R_n and R'_n[a] (m)	64.1	64.4	70.4	64.8	64.8

[a]Inferred from optimization.

[31] There are $2N + 2$ measurements and $3N$ parameters to be fitted. Thus, additional restrictions on the parameter values need to be specified in order to produce an overconstrained set of equations suitable for optimization. We suppose initially that $R'_n = R_n$ and then consider the implications of alternative assumptions. Optimization was carried out using SOLVER in Microsoft Excel [*Fylstra et al.*, 1998], which uses a generalized reduced gradient method for nonlinear problems, giving a maximum absolute relative error in m_n, Q_n, s_w, and s'_w of 1.0×10^{-3}, with reduced gradients of zero reported for each variable. The results are summarized in Table 2. The optimized values of Q'_n suggest that vertical flow in the borehole is fed from levels 1 to 3 whereas levels 4 to 6 act as sinks. The optimized radii of influence are in a range consistent with field data: during the tracer test, significant drawdown was observed in a borehole with similar construction to the test boreholes at a distance of 20 m from the abstraction, but no drawdown was recorded in an additional borehole at approximately 85 m. The Thiem analysis of a steady state, constant discharge test conducted in BH3 [*Ferguson*, 2006], which included the aquifer layer that was isolated from the test zone in the tracer test, gives a transmissivity of 54 m^2 d^{-1} and a radius of influence of 50 m. Data from the same study show that the total conductance of the tracer test zone represents just 48% of that of the entire open borehole (Table 1), which assuming similar radii of influence in the test zone and above, suggests a transmissivity for the tracer test zone of about 26 m^2 d^{-1}. This is in close agreement with the total transmissivity of 24 m^2 d^{-1} inferred from the tracer test analysis. Conductance values for individual levels predicted from the inferred hydraulic parameters show a RMSE of 2.7 m^2 d^{-1} compared with those values shown in Table 1. This error is dominated by a large difference of 4.23 m^2 d^{-1} between the measured conductance and that derived for layer 6, without which the RMS drops to 1.4 m^2 d^{-1}. Since $|Q'_n| \ll |Q_n|$ for all n, the correlation between the inferred transmissivity and the abstraction rate in each layer is high (1.000 correct to 3 decimal places).

[32] The assumption that $R'_n = R_n$ can be evaluated by considering the sensitivity of the optimized values of T_n and R_n to values of R'_n for given values of the other parameters. Solving equation (1) and equation (2) for T_n and R_n shows that the optimized value of T_n is independent of R'_n and that the optimized value of R_n can be expressed as

$$\ln R_n = A + B \ln R'_n, \tag{25}$$

where A and B are functions of the remaining parameters. Thus, for a particular layer, and using $R'_n = R_n$ as the base case, equation (25) can be used to assess the change in the optimized value of R_n, given alternative assumptions about R'_n. Figure 6 shows these changes as a function of R'_n for the parameter values associated with the tracer test. The changes are minor and show that for this particular data set, the optimization is comparatively insensitive to assumptions relating to R'_n.

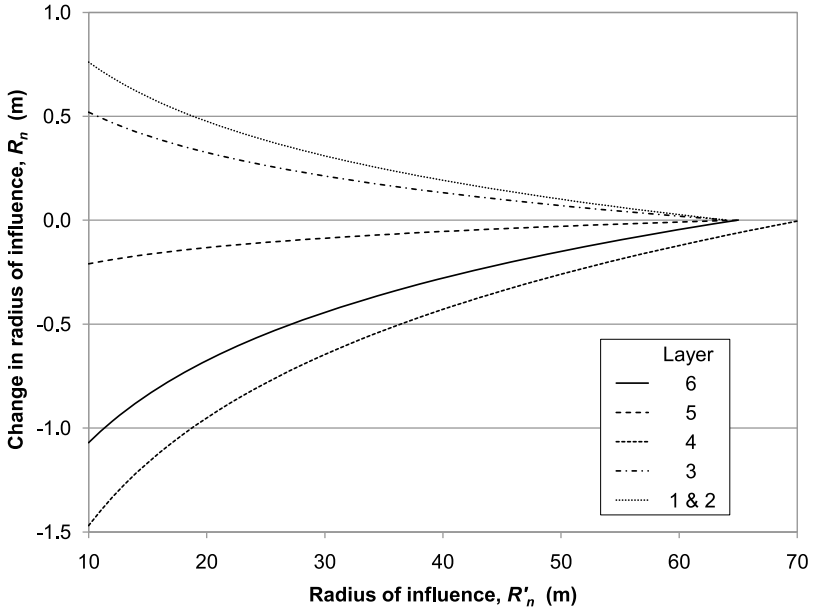

Figure 6. Changes in the optimized values of R_n, as a function of R'_n, from those estimated using $R'_n = R_n$.

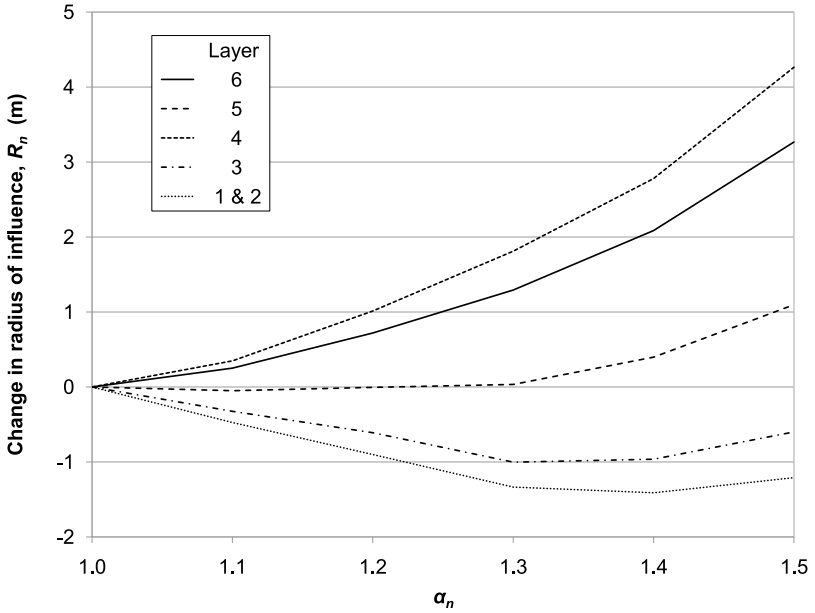

Figure 7. Changes in the optimized values of R_n, as a function of α_n, from those using $\alpha_n = 1$.

[33] Figure 7 shows the change in inferred radius of influence for each layer from its original value as a function of α_n. Changing the values of α_n for individual layers produces smaller changes. Inferred transmissivity values are relatively insensitive to changes in α_n, showing a maximum absolute change of 2.6% and a mean absolute change of 0.7% of their original values over the range of α_n tested.

5. Discussion: Importance of Vertical Flow

5.1. Effect of Vertical Head Gradients

[34] The forced gradient, convergent tracer test described above is a useful vehicle for illustrating the sensitivity of tracer recovery to the model parameters. Throughout section 5, we assume in calculations that the values of α_n are all equal to one as estimated from the field data, the system is mass conservative, the boreholes are of equal diameter, and that $R'_n = R_n$ for all n.

[35] The effect of vertical head gradients on tracer test results can be illustrated by comparing the fraction of total mass recovery and the pattern of vertical flow in the injection borehole reported above with those calculated for two hypothetical tests; one under the substantially greater vertical head gradients prevailing in 2006 (Table 1), and another in which background heads are assumed to have equilibrated. The pumping rate is taken to be unchanged in both scenarios and the inferred transmissivity values and radii of influence given in Table 2 are assumed to apply. Equations (12) and (13) are used to estimate Q_n, and Q'_n, and mass recovery is calculated using equations (17) and (18).

[36] The results for the hypothetical test in 2006, summarized in Table 3, show that the pattern of upflow in the injection borehole is qualitatively unchanged, but that the magnitude is much greater than in the 2008 test. There are relatively minor changes in the distribution of flow to the abstraction borehole, but most significantly, 64% of the tracer transport takes place in the highest layer and there is no tracer recovery at all in the lowest three aquifer layers.

[37] For the case in which the background vertical head gradients are zero, the simulation results (Table 4) indicate a change in the pattern of vertical flow in the injection borehole from the 2008 test. In this case, pumping induces vertical flows toward the central section of the borehole with the major inflows to the borehole occurring in the lower layers. This pattern results in a tracer recovery in layer 4 approximately 2.8 times greater than that expected from considerations of transmissivity alone.

5.2. Comparison With a Previous Tracer Test

[38] A tracer test, in which a tracer was sampled just from the discharge from the abstraction borehole, was conducted as part of a previous investigation in 2005 [*Joyce et al.*, 2007]. This test was carried out with the direction of flow reversed and without the packer in BH3 (Figure 1). Thus, when BH3 was pumped, groundwater was abstracted from layers 1 to 6 and from the (unconfined) aquifer above. The test was conducted at an abstraction rate of 210 m^3 d^{-1}. Fluorescein mass recovery is estimated to be 67% of the 20 g injected. The fluorescein breakthrough curve from the top of layer 6 in the 2008 test, standardized to have unit area (Figure 8), shows significant differences in shape from that from the 2005 test (Figure 10). We speculate here that the differences in the curves might be explained by different

Table 3. Mass Recovery and Flow to Boreholes Assuming Background Heads Measured in 2006

	Aquifer Layer				
	1, 2	3	4	5	6
Fraction of mass recovered	0.0	0.0	0.08	0.28	0.64
Abstraction rate Q_n (m^3 d^{-1})	43	22	9	36	13
Flow to injection borehole due to vertical flow Q'_n (m^3 d^{-1})	5.71	2.09	−0.59	−2.20	−5.01
Ω_n	11.75	8.77	−7.29	−6.60	−62.5

Table 4. Mass Recovery and Flow to Boreholes Assuming Zero Background Head Gradient

	Aquifer Layer				
	1, 2	3	4	5	6
Fraction of mass recovered	0.23	0.13	0.21	0.29	0.14
Abstraction rate Q_n (m^3 d^{-1})	37	20	9	38	18
Flow to injection borehole due to vertical flow Q'_n (m^3 d^{-1})	0.054	0.019	−0.083	0.008	0.003
Ω_n	0.14	0.09	−0.91	0.02	0.01

patterns of vertical flow in the injection borehole during the two tests.

[39] Although the total abstraction rate during the 2005 test is known, the resulting discharge from layers 1 to 6 is not since a proportion of the water abstracted is drawn from the overlying unconfined aquifer. Furthermore, there are no available data relating to ambient vertical head gradients in 2005. Nevertheless, an insight into the 2005 test can be obtained by considering the results of simulations using the results of the 2008 test and the parameterized model of recovery from section 4.3. We assume, for the sake of argument, that the ambient vertical gradients are the same as those prevailing in 2006. In the absence of pumping, these conditions produce outflow to layer 6 from both boreholes (Table 1). Hence, $Q'_6 < 0$ and, significantly, $Q_6 < 0$. To recover tracer in BH3 from layer 6, the borehole must be pumped at a rate sufficient to reverse this outflow. The parameterized model predicts Q_6 to be zero when the total discharge from layers 1 to 6 is approximately 34 m^3 d^{-1} in which case recovery occurs only in layers 4 and 5 since the stagnation points in layers 1 to 3 lie between the boreholes. At this pumping rate the model predicts recovery in layers 4 and 5 to be approximately in the ratio 1:4. Figure 9 shows the breakthrough curves from layers 4 to 6 in the 2008 test. Figure 10 shows the 2005 breakthrough curve and a hypothetical breakthrough curve constructed from the combined breakthrough curves from layers 4 and 5 in the 2008 test, weighted so that the mass recoveries are in the predicted ratio. Both curves have been standardized to have unit area so that their shapes can be simply compared. Since the modeled ratios of Q_4 to Q_5 are almost identical for 2005 and 2008, the 2008 discharges through layers 4 and 5 have been scaled by the same factor to give a visual fit to the 2005 breakthrough curve, which is remarkably good. Increasing the discharge from layers 1 to 6 beyond 34 m^3 d^{-1} increases the influence of layer 6 on the hypothetical breakthrough curve, changing its shape. For discharges from approximately 34 m^3 d^{-1} to 68 m^3 d^{-1}, the flow stagnation point lies on the far side of the abstraction borehole from the injection borehole (case 4), so only a proportion of the tracer from the injection borehole is recovered, which is qualitatively consistent with the lower recovery in the 2005 test.

[40] Drawing firm conclusions from the foregoing discussion has to be approached with some care since the quality of the data upon which it is based is poor and the scaling of arrival times has been based upon quality of fit rather than on calculation. Thus, conclusions remain speculative. However, the similarity of the breakthrough curves in Figure 10 would appear to suggest that breakthrough from layers 4 and 5 dominated the 2005 test, highlighting the potential importance of vertical flow in the injection borehole and the consequent necessity to ensure that the abstraction rate applied during such a test is adequate.

5.3. Scale of Tracer Experiments

[41] The fundamental control on recovery in each layer is the position of the flow stagnation point. In the region of the injection borehole the stagnation point is characterized by $rQ'_n/(\alpha_n Q_n + Q'_n)$. For small values of rQ'_n or large values of Q_n, the stagnation point is close to the center of the borehole. Since $r > 0$ and Q_n is finite, a stagnation point exactly at the center of the injection borehole indicates that $Q'_n = 0$, and consequently that the horizontal discharge

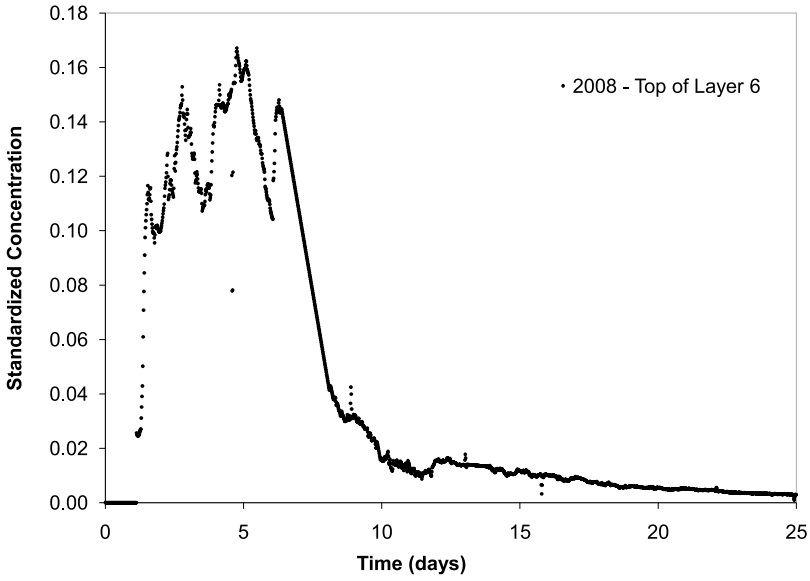

Figure 8. Scaled breakthrough curve as sampled from the top of layer 6 (i.e., through the main pump) in the 2008 tracer test.

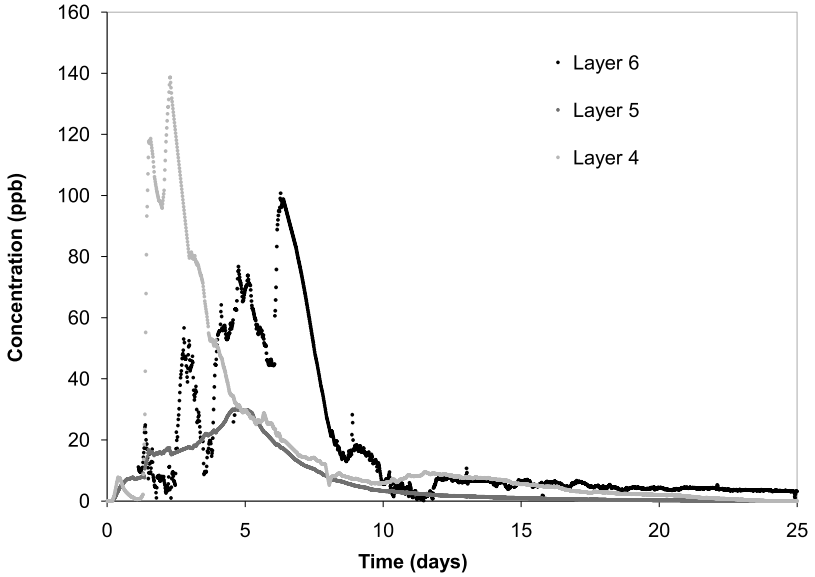

Figure 9. Breakthrough curves for layers 4, 5, and 6 from the tracer test conducted in 2008.

through it, and hence the recovery, is proportional to the layer transmissivity. Thus, if r is sufficiently small or Q_n sufficiently large for all n, recovery is effectively proportional to transmissivity.

[42] For large interborehole distances, the proportional recovery in each layer can be estimated in general by letting r increase without limit in equation (18). Since there is no recovery when $Q_n \leq 0$, we assume that Q_n is positive which gives the following: when $Q'_n > 0$, recovery tends to zero; when $-Q_n < Q'_n < 0$ recovery becomes proportional to $-Q'_n$; and when $Q'_n < -Q_n$ recovery becomes proportional to Q_n.

[43] The effect of the scale of the tracer test can be illustrated by considering the three scenarios outlined in section 5.1, namely, the hypothetical test in 2006, the 2008 tracer test with reduced vertical head gradients, and a test with background vertical head gradients of zero. When the background vertical head gradients are large as in the hypothetical 2006 test, recovery is dominated by vertical flows and is almost independent of the interborehole distance: the value of r has to be reduced to less than 1.5 m before a change in the third significant figure of fractional tracer recovery can be seen. Figure 11 shows the distribution of recovery as a function of r based upon the smaller range of vertical head values from the 2008 tracer test. In the limit as r reduces, the recovery reflects the transmissivity distribution (not shown). As r increases, the recovery from the layers in which there is inflow to the injection borehole due to vertical flow reduces to zero, and the layers in which there is outflow show recovery that is proportional to Q'_n.

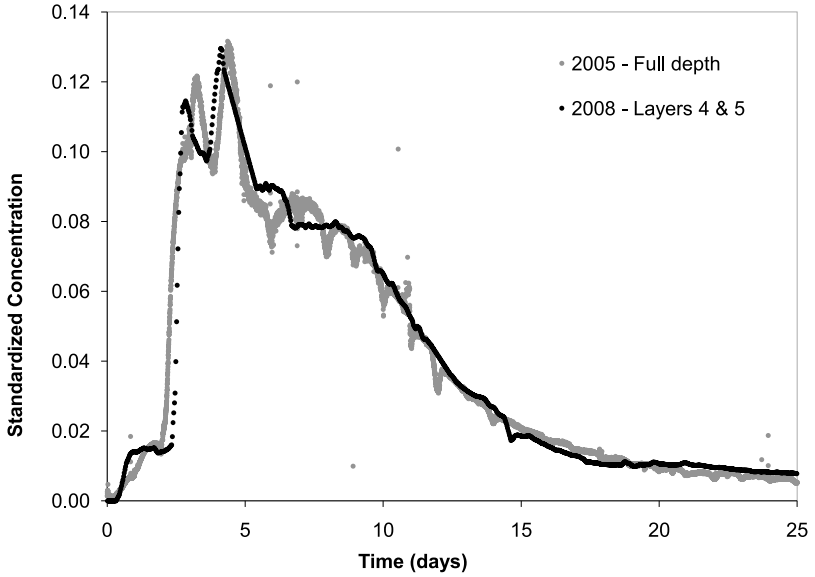

Figure 10. Scaled fluorescein breakthrough curves for tracer test conducted in 2005 and the weighted average of layers 4 and 5 only from the test in 2008.

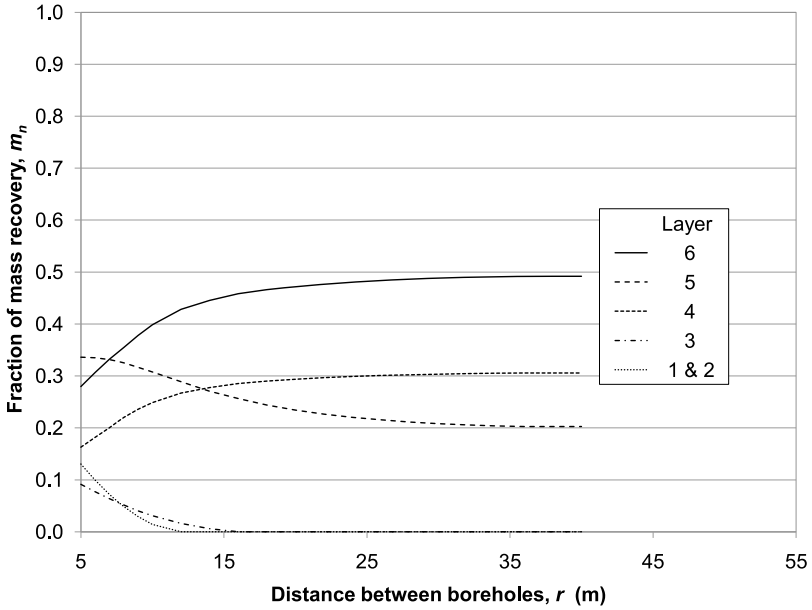

Figure 11. Fraction of total mass recovery in each layer as a function of the interborehole distance based upon the background head distribution assumed to prevail during the 2008 tracer test.

Figure 12 shows the scenario in which the background vertical gradients are zero. In this case, the progression from transmissivity to vertical flow dominance with distance is slower than in the previous scenarios. Only layer 4 exhibits outflow from the injection borehole. This layer happens to be the least transmissive, and so for small values of r, it shows the lowest recovery, but in larger-scale tests it provides the principal pathway for tracer migration.

5.4. Sensitivity of Recovery to Radii of Influence

[44] The issue of layer 4 in scenario 3 in section 5.3 (zero background vertical head gradients) is worthy of further attention. In this scenario, if all the radii of influence are equal, the recovery is independent of the interborehole distance and is proportional to the transmissivity. So, the behavior exhibited in Figure 12 is due entirely to the distribution of the radii of influence. In this particular scenario, the radius of influence in layer 4 is greater than those in other layers, albeit by less than 10%, in order to match the large recovery observed in the field test (Figure 5). In general, variations in radii of influence of at least similar magnitudes are likely to occur commonly in the field, and these can have a significant impact on the distribution of tracer recovery. For example, reducing R_4 and R'_4 in scenario 3 from 70.4 m to 68.9 m creates flow from the

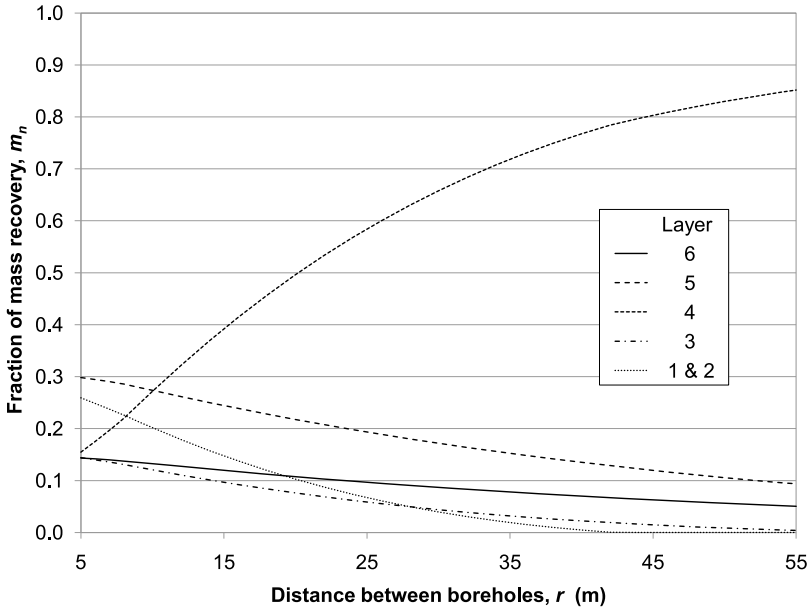

Figure 12. Fraction of total mass recovery in each layer as a function of the interborehole distance based upon background vertical head gradients of zero.

injection borehole in layer 6, and reducing it again to 68.4 m creates additional flow from the borehole in layer 5. At a value of 66.1 m the recovery in layer 5 becomes larger than that in layer 4 in a test conducted between boreholes 40 m apart.

[45] The use of the radius of influence needs to be treated with some caution since it is a device based upon the Thiem analysis that is used to describe the size of the cone of depression due to an abstraction at late times when a quasi-steady state has been achieved. Mathematically, its use implies an unphysical change in the hydraulic gradient at the radius of influence, effectively imposing a fixed head boundary condition on the abstraction. Thus, it is inappropriate to overinterpret the drawdown close to the radius of influence. Nevertheless, nearer the abstraction borehole, the parameterized Thiem analysis, including the radius of influence, is widely accepted as characterizing the later time cone of depression well.

[46] This sensitivity to the radii of influence highlights the importance of the observation that conservative tracer recovery is limited by the hydraulic regime at the injection borehole. The flow through the injection borehole due to pumping is often small since it is inversely proportional to the scale of the test, and consequently, minor differences in Q'_n created by subtle variations in the radii of influence between layers, can have a major impact on the vertical distribution of tracer recovery.

5.5. Implications for the Design and Interpretation of Tracer Tests

[47] Tracer tests are conducted for a variety of reasons. We consider tests that are carried out in order to develop our understanding of transport processes, which use the aquifer as a field laboratory, and those whose purpose is to characterize the contaminant transport properties of an aquifer itself. In both cases, the foregoing analysis shows that without depth-dependent monitoring and hydraulic testing, we may easily be mistaken about the layers in the aquifer that are actually being investigated. In the first kind of test, provided we have suitable measurements, we can make valid inferences about transport processes on the basis of knowledge of the mass of tracer that passes through each layer. In the second type of test, taking just depth-integrated samples from the abstraction borehole can lead to a fundamental misunderstanding about the transport behavior of the aquifer under natural head gradients. The discussion of scenario 3 in section 5.3 shows that under unfavorable conditions, it is possible for transport during the test to be focused in a single, low-transmissivity layer that would play only a minor role in contaminant migration driven by natural horizontal head gradients. In general, controls on transport during a tracer test include a scale-dependent combination of transmissivity values, radii of influence, and background heads. There is, therefore, a potential problem in applying results from this kind of tracer test to studies of migration under natural head gradients in which the transmissivity distribution plays a dominant part.

[48] When $Q_n < -Q'_n$, recovery in layer n is incomplete (cases 4 and 5). When $Q_n > -Q'_n$ and $\Omega_n \leq -1$ (case 3) the recovery in layer n is determined entirely by the vertical flow in the injection borehole and when $\Omega_n \geq -1$ (case 1) the recovery is zero. Thus, to ensure recovery and reduce the sensitivity of recovery to vertical flow in the injection borehole, the scale of the test and discharge in each layer should be such that $-1 < \Omega_n < 1$, with Ω_n as close to zero as practical.

6. Summary and Conclusions

[49] Theoretical models have been presented that describe the steady state flows and relative tracer mass recovery in a borehole to borehole forced gradient tracer test in a multilayered aquifer system, including the effect of background vertical head gradients. Steady state drawdown in each borehole is also given. The models have been applied to the results from a tracer test and a range of hydraulic tests in a sandstone aquifer. Using a simple optimization procedure, the transmissivity and steady state radius of influence of each layer in the system have been inferred from the tracer mass recovery data. The inferred hydraulic properties have been shown to be consistent with the known hydraulic behavior of the system and the underlying model used to reinterpret a previous tracer test at the site.

[50] Further analysis of the forced gradient test shows that tracer recovery in each layer is sensitive to the vertical distribution of head and to the scale of the test. In particular, as the scale of the test increases, recovery becomes progressively more sensitive to vertical flows in the injection borehole. If the aquifer is heterogeneous in the vertical, small vertical flows will be produced through pumping even when the natural vertical gradients are zero, and these small flows can be sufficient to dominate the distribution of recovery in the vertical. These results highlight the difficulty in extrapolating tracer test results in multilayered systems to contaminant migration under natural gradients. Furthermore, prediction of recovery is inherently uncertain since it depends strongly upon the hydraulic behavior of the aquifer in the immediate vicinity of the injection borehole, which is likely to be influenced by local small-scale heterogeneities, particularly in fractured rock.

[51] Horizontal head gradients, which are not included in the models presented, have the potential to change the vertical distribution of recovery and may play a role in the inference of hydraulic property values. We would expect the effects of horizontal gradients to be most significant when the abstraction rate is too small to dominate the flow field or when the stagnation point lies within the injection borehole. However, quantifying the scale of the impacts of these gradients on the distribution of recovery is not straightforward without theoretical models that include them. Unfortunately, the development of such models is beyond the scope of this paper and remains a challenge for the future.

[52] Nevertheless, the theoretical models presented here are a quantitative aid to the design and interpretation of tracer tests, and can be used to highlight and minimize the uncertainties inherent in the design process. In particular, the models can form the basis of a quantitative assessment of the scale of test and pumping rate required to avoid problems of the biased sampling of aquifer layers in a proposed tracer test. The models might also be applied to other investigations conducted near pumping wells in multilayered aquifers such as point dilution tests and water quality sampling.

[53] **Acknowledgments.** This work was carried out as part of the SWITCH project funded by the European Union under the Sixth Framework Programme. The borehole research site was set up initially

with funding from the Engineering and Physical Sciences Research Council. We would like to thank the three anonymous reviewers for their valuable comments on the manuscript.

References

Allen, D. J., L. J. Brewerton, L. M. Coleby, B. R. Gibbs, M. A. Lewis, A. M. MacDonald, S. J. Wagstaff, and A. T. Williams (1997), The physical properties of major aquifers in England and Wales, *Tech. Rep. WD/97/34*, 312 pp., Br. Geol. Surv., London.

Bouch, J. E., E. Hough, S. J. Kemp, J. A. McKervey, G. M. Williams, and R. B. Greswell (2006), Sedimentary and diagenetic environments of the Wildmoor Sandstone Formation (UK): Implications for groundwater and contaminant transport, and sand production, in *Fluid Flow and Solute Movement in Sandstones: The Onshore UK Permo-Triassic Red Bed Sequence*, edited by R. D. Barker and J. H. Tellam, *Geol. Soc. Spec. Publ.*, *263*, 129–158.

Brassington, F. C. (1992), Measurements of head variations within observation boreholes and their implications for groundwater monitoring, *J. Inst. Water Environ. Manage.*, *6*(3), 91–100, doi:10.1111/j.1747-6593.1992.tb00742.x.

Clarkson, M. H., D. Birks, P. L. Younger, A. Carter, and S. Cone (2009), Groundwater cooling at the Royal Festival Hall, London, *Q. J. Eng. Geol. Hydrogeol.*, *42*, 335–346, doi:10.1144/1470-9236/08-080.

Ferguson, H. A. (2006), Determining the hydraulic characteristics of the Wildmoor Sandstone formation and evaluating the condition of the study site, MSc thesis, Univ. of Birmingham, Birmingham, U. K.

Flynn, R. M., P. A. Schnegg, R. Costa, G. Mallen, and F. Zwahlen (2005), Identification of zones of preferential groundwater tracer transport using a mobile downhole fluorometer, *Hydrogeol. J.*, *13*(2), 366–377, doi:10.1007/s10040-004-0388-3.

Furlong, B. V., M. S. Riley, A. W. Herbert, J. A. Ingram, R. Mackay, and J. H. Tellam (2011), Using regional groundwater flow models for prediction of regional wellwater quality distributions, *J. Hydrol.*, *398*(1–2), 1–16, doi:10.1016/j.jhydrol.2010.11.022.

Fylstra, D., L. Lasdon, J. Watson, and A. Waren (1998), Design and use of the Microsoft Excel Solver, *Interfaces*, *28*(5), 29–55, doi:10.1287/inte.28.5.29.

Gierczak, R. F. D., J. F. Devlin, and D. L. Rudolph (2006), Combined use of field and laboratory testing to predict preferred flow paths in an heterogeneous aquifer, *J. Contam. Hydrol.*, *82*(1–2), 75–98, doi:10.1016/j.jconhyd.2005.09.002.

Gutiérrez, M. G., J. Guimerà, A. Y. de Llano, A. H. Benitez, J. Humm, and M. Saltink (1997), Tracer test at El Berrocal site, *J. Contam. Hydrol.*, *26*(1–4), 179–188, doi:10.1016/S0169-7722(96)00067-8.

Hartmann, S., N. E. Odling, and L. J. West (2007), A multi-directional tracer test in the fractured Chalk aquifer of E. Yorkshire, UK, *J. Contam. Hydrol.*, *94*(3–4), 315–331, doi:10.1016/j.jconhyd.2007.07.009.

Hitchmough, A. M., M. S. Riley, A. W. Herbert, and J. H. Tellam (2007), Estimating the hydraulic properties of the fracture network in a sandstone aquifer, *J. Contam. Hydrol.*, *93*(1–4), 38–57, doi:10.1016/j.jconhyd.2007.01.012.

Joyce, E., J. Rueedi, A. Cronin, S. Pedley, J. H. Tellam, and R. B. Greswell (2007), Fate and transport of phage and viruses in UK Permo-Triassic sandstone aquifers, *Sci. Rep. SC030217/SR*, 89 pp., Environ. Agency, London.

Joyce, E., et al. (2008), Assessing the hazard from viruses in waste-water recharge of urban sandstone aquifers, in *Groundwater Quality 2007: Securing Groundwater Quality in Urban and Industrial Environments*, IAHS Press, Wallingford, U. K.

Karasaki, K., B. Freifeld, A. Cohen, K. Grossenbacher, P. Cook, and D. Vasco (2000), A multidisciplinary fractured rock characterization study at Raymond field site, Raymond, CA, *J. Hydrol.*, *236*(1–2), 17–34, doi:10.1016/S0022-1694(00)00272-9.

Kurtzman, D., R. Nativ, and E. M. Adar (2005), The conceptualization of a channel network through macroscopic analysis of pumping and tracer tests in fractured chalk, *J. Hydrol.*, *309*(1–4), 241–257, doi:10.1016/j.jhydrol.2004.11.023.

Le Borgne, T., et al. (2007), Comparison of alternative methodologies for identifying and characterizing preferential flow paths in heterogeneous aquifers, *J. Hydrol.*, *345*(3–4), 134–148, doi:10.1016/j.jhydrol.2007.07.007.

Lloyd, J. W., R. Greswell, G. M. Williams, R. S. Ward, R. Mackay, and M. S. Riley (1996), An integrated study of controls on solute transport in the Lincolnshire limestone, *Q. J. Eng. Geol.*, *29*, 321–339, doi:10.1144/GSL.QJEGH.1996.029.P4.06.

Mathias, S. A., A. P. Butler, D. W. Peach, and A. T. Williams (2007), Recovering tracer test input functions from fluid electrical conductivity logging in fractured porous rocks, *Water Resour. Res.*, *43*, W07443, doi:10.1029/2006WR005455.

McCarthy, J. F., B. Gu, L. Liang, J. MasPla, T. M. Williams, and T. C. J. Yeh (1996), Field tracer tests on the mobility of natural organic matter in a sandy aquifer, *Water Resour. Res.*, *32*(5), 1223–1238, doi:10.1029/96WR00285.

Price, V. (2008), Field experiments on the movement of viruses through sandstone, MSc thesis, Univ. of Birmingham, Birmingham, U. K.

Ptak, T., and G. Schmid (1996), Dual-tracer transport experiments in a physically and chemically heterogeneous porous aquifer: Effective transport parameters and spatial variability, *J. Hydrol.*, *183*(1–2), 117–138, doi:10.1016/S0022-1694(96)80037-0.

Ptak, T., M. Piepenbrink, and E. Martac (2004), Tracer tests for the investigation of heterogeneous porous media and stochastic modelling of flow and transport—A review of some recent developments, *J. Hydrol.*, *294*(1–3), 122–163, doi:10.1016/j.jhydrol.2004.01.020.

Reimus, P. W., M. J. Haga, A. I. Adams, T. J. Callahan, H. J. Turin, and D. A. Counce (2003a), Testing and parameterizing a conceptual solute transport model in saturated fractured tuff using sorbing and nonsorbing tracers in cross-hole tracer tests, *J. Contam. Hydrol.*, *62–63*, 613–636, doi:10.1016/S0169-7722(02)00185-7.

Reimus, P., G. Pohll, T. Mihevc, J. Chapman, M. Haga, B. Lyles, S. Kosinski, R. Niswonger, and P. Sanders (2003b), Testing and parameterizing a conceptual model for solute transport in a fractured granite using multiple tracers in a forced-gradient test, *Water Resour. Res.*, *39*(12), 1356, doi:10.1029/2002WR001597.

Riley, M. S., R. S. Ward, and R. B. Greswell (2001), Converging flow tracer tests in fissured limestone, *Q. J. Eng. Geol. Hydrogeol.*, *34*, 283–297, doi:10.1144/qjegh.34.3.283.

Ronen, D., M. Magaritz, and F. J. Molz (1991), Comparison between natural and forced gradient tests to determine the vertical distribution of horizontal transport properties of aquifers, *Water Resour. Res.*, *27*(6), 1309–1314, doi:10.1029/91WR00332.

Rushton, K. R., and S. Salmon (1993), Significance of vertical flow-through low-conductivity zones in Bromsgrove sandstone aquifer, *J. Hydrol.*, *152*(1–4), 131–152, doi:10.1016/0022-1694(93)90143-W.

Segar, D. A. (1993), The effect of open boreholes on groundwater flow and chemistry, Ph.D. thesis, Univ. of Birmingham, Birmingham, U. K.

Stagg, K. A., J. H. Tellam, M. H. Barrett, and D. N. Lerner (1998), Hydrochemical variations with depth in a major UK aquifer: The fractured, high permeability Triassic Sandstone, in *Gambling With Groundwater—Physical, Chemical, and Biological Aspects of Aquifer-Stream Relations*, edited by J. V. Brahana et al., pp. 53–58, Am. Inst. of Hydrol., St. Paul, Minn.

Streetly, H. R., A. C. L. Hamilton, C. Betts, J. H. Tellam, and A. W. Herbert (2002), Reconnaissance tracer tests in the Triassic sandstone aquifer north of Liverpool, UK, *Q. J. Eng. Geol. Hydrogeol.*, *35*, 167–178, doi:10.1144/1470-9236/2000-30.

Taylor, R., C. Tindimugaya, J. Barker, D. Macdonald, and R. Kulabako (2010), Convergent radial tracing of viral and solute transport in gneiss saprolite, *Ground Water*, *48*(2), 284–294, doi:10.1111/j.1745-6584.2008.00547.x.

Taylor, R. G., A. A. Cronin, S. A. Trowsdale, O. P. Baines, M. H. Barrett, and D. N. Lerner (2003), Vertical groundwater flow in Permo-Triassic sediments underlying two cities in the Trent River Basin (UK), *J. Hydrol.*, *284*(1–4), 92–113, doi:10.1016/S0022-1694(03)00276-2.

Tellam, J. H., and R. D. Barker (2006), Towards prediction of saturated-zone pollutant movement in groundwaters in fractured permeable-matrix aquifers: The case of the UK Permo-Triassic sandstones, in *Fluid Flow and Solute Movement in Sandstones: The Onshore UK Permo-Triassic Red Bed Sequence*, edited by R. D. Barker and J. H. Tellam, *Geol. Soc. Spec. Publ.*, *263*, 1–48.

West, L. J., and N. E. Odling (2007), Characterization of a multilayer aquifer using open well dilution tests, *Ground Water*, *45*(1), 74–84, doi:10.1111/j.1745-6584.2006.00262.x.

M. F. Aller, Centre for Sustainable Water Management, Lancaster Environment Centre, Lancaster LA1 4AP, UK.

V. Durand, Laboratoire Interactions et Dynamique des Environnements de Surface, UMR 8148, Université Paris–Sud XI, CNRS, F-91405 Orsay CEDEX, France.

R. B. Greswell, M. S. Riley, and J. H. Tellam, Water Sciences, School of Geography, Earth and Environmental Sciences, University of Birmingham, Birmingham B15 2TT, UK. (m.riley@bham.ac.uk)